

Calibrating Multimodal Consensus for Emotion Recognition

Guowei Zhong, Junjie Li, *Member, IEEE*, Huaiyu Zhu, *Member, IEEE*, Ruohong Huan, and Yun Pan, *Member, IEEE*

Abstract—In recent years, Multimodal Emotion Recognition (MER) has made substantial progress. Nevertheless, most existing approaches neglect the semantic inconsistencies that may arise across modalities, such as conflicting emotional cues between text and visual inputs. Besides, current methods are often dominated by the text modality due to its strong representational capacity, which can compromise recognition accuracy. To address these challenges, we propose a model termed Calibrated Multimodal Consensus (CMC). CMC introduces a Pseudo Label Generation Module (PLGM) to produce pseudo unimodal labels, enabling unimodal pretraining in a self-supervised fashion. It then employs a Parameter-free Fusion Module (PFM) and a Multimodal Consensus Router (MCR) for multimodal finetuning, thereby mitigating text dominance and guiding the fusion process toward a more reliable consensus. Experimental results demonstrate that CMC achieves performance on par with or superior to state-of-the-art methods across four datasets, CH-SIMS, CH-SIMS v2, CMU-MOSI, and CMU-MOSEI, and exhibits notable advantages in scenarios with semantic inconsistencies on CH-SIMS and CH-SIMS v2. The implementation of this work is publicly accessible at <https://github.com/gw-zhong/CMC>.

Index Terms—Multimodal emotion recognition, multimodal fusion, multimodal learning, modality semantic inconsistency.

I. INTRODUCTION

WITH the rapid growth of social media, users' emotional expressions have become increasingly diverse, evolving from traditional text-based formats to multimodal video content that incorporates text, audio, and visual elements. Multimodal Emotion Recognition (MER) seeks to integrate information from these heterogeneous modalities to more accurately identify human emotions, making it a key task in affective computing.

Despite the extensive research conducted in the MER field, including studies on multimodal fusion [1]–[8], modality missingness [9]–[15], and out-of-distribution generalization [16]–[20], most methods still suffer from two major limitations.

This work was supported by the National Key R&D Program of China (2023YFC3603102), the “Pioneer” and “Leading Goose” R&D Program of Zhejiang (2024C03027), and the National Natural Science Foundation of China (62306272). (Corresponding author: Yun Pan.)

Guowei Zhong, Junjie Li, Huaiyu Zhu, Yun Pan are with the College of Information Science and Electronic Engineering, Zhejiang University, Hangzhou, 310027, China (E-mail: gwzhong@zju.edu.cn, lijunjie_isee2019@zju.edu.cn, zhuhuaiyu@zju.edu.cn, panyun@zju.edu.cn).

Ruohong Huan is with the College of Computer Science and Technology, Zhejiang University of Technology, Hangzhou, 310023, China (E-mail: huanrh@zjut.edu.cn).

Junjie Li is also with Zhejiang University Jinhua Research Institute, Jinhua, 321000, China.

This work has been submitted to the IEEE for possible publication. Copyright may be transferred without notice, after which this version may no longer be accessible.

First, they neglect potential semantic inconsistencies across modalities. Second, because text features typically rely on pretrained language models (e.g., BERT [21]), whereas audio and visual modalities often depend on traditional handcrafted features, models are frequently dominated by the text modality, whose stronger representational capacity can adversely affect overall recognition performance.

Therefore, the key challenge lies not in simply performing multimodal fusion, but in establishing a reliable multimodal consensus in which all modalities contribute collaboratively without being dominated by the strongest one.

As shown in Fig. 1, even with the inclusion of audio and visual modalities, existing method struggles to make accurate predictions when faced with semantic inconsistencies across modalities. In two video clips from the CH-SIMS [22] dataset, the multimodal emotions expressed by the characters conflict with the text unimodal emotions. Taking EMT-DLFR [13] as an example, because the representational power of text features derived from pretrained language models far exceeds that of audio and visual features based on handcrafted descriptors, the model is incorrectly dominated by the text modality in the examples shown in Fig. 1. As a result, it disregards the modalities that correctly convey the emotions and ultimately produces recognition errors. Moreover, the prediction results show that although incorporating audio and visual information alongside text can partially mitigate the dominance of the text modality and move the prediction closer to the correct multimodal label, the weak representational capacity of the audio and visual modalities still prevents the model from accurately identifying emotions.

Overall, existing MER approaches typically frame multimodal learning as a feature fusion task, implicitly assuming that all modalities contribute consistently. In practice, however, modalities in MER may convey conflicting cues, and naive fusion often amplifies the effects of dominant or noisy modalities. As a result, prior methods struggle to establish a genuine multimodal consensus in which the final decision reflects balanced and reliable contributions from all modalities.

To address these challenges, we propose the Calibrated Multimodal Consensus (CMC) model, which redefines the objective of MER as establishing a calibrated multimodal consensus rather than relying on naive fusion. The CMC model comprises two stages and three modules. In the first stage, the Pseudo Label Generation Module (PLGM) produces pseudo unimodal labels to enable unimodal pretraining in a self-supervised manner. In the second stage, the Parameter-free Fusion Module (PFM) performs modality fusion while preserving

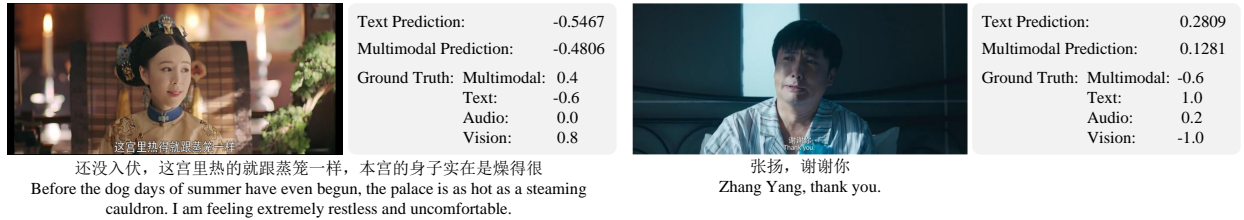


Fig. 1. Two examples of recognition errors caused by semantic conflicts between modalities in the CH-SIMS dataset for EMT-DLFR. “Text Prediction” refers to results obtained using only the text modality, whereas “Multimodal Prediction” refers to results obtained using all three modalities. Note: In the CH-SIMS dataset, the annotated emotional polarity ranges from -1 to 1 , with smaller values indicating more negative emotions.

the original semantic information of each modality. Finally, the Multimodal Consensus Router (MCR) automatically adjusts the confidence weights of modality-specific predictions to achieve an accurate multimodal consensus.

In summary, the main contributions of this paper are as follows:

- We propose a novel calibrated consensus model, CMC, which effectively mitigates the challenges of semantic inconsistency across modalities and text modality dominance.
- Within CMC, we design the PLGM to generate pseudo labels for each modality based on gradients and to enable unimodal pretraining in a self-supervised manner. We introduce the PFM to perform multimodal fusion without additional parameters while preserving the semantic information of the original modalities. We further propose the MCR, which automatically assigns adaptive weights to modality-specific predictions to achieve an accurate multimodal consensus.
- CMC achieves performance on par with or superior to state-of-the-art methods across four datasets, CH-SIMS, CH-SIMS v2, CMU-MOSI, and CMU-MOSEI, and demonstrates notable advantages in handling semantic inconsistencies on CH-SIMS and CH-SIMS v2.

II. RELATED WORK

A. Multimodal Fusion

In traditional MER, researchers primarily focused on developing effective fusion strategies.

Tsai et al. [23] introduced the Multimodal Transformer (MuLT), which extends the Transformer architecture [24] by incorporating cross-modal and self-attention to model interactions both within and across modalities. Lv et al. [25] proposed a message hub that separately stores multimodal information and employs a progressive strategy to facilitate cross-modal interactions across Transformer layers. Liang et al. [26] highlighted that distribution mismatches between modality-specific features could reduce the effectiveness of cross-modal attention and therefore proposed a modality-invariant cross-modal attention mechanism to mitigate such differences. To address the high computational cost of MuLT, Cheng et al. [27] introduced the Sparse Phased Block (SP-Block) to sample long sequences and further reduced complexity by employing a shared attention matrix for multimodal interactions. Guo et al. [28] developed a method that dynamically adjusts word

embeddings using information from non-linguistic modalities. Yang et al. [29] proposed a fusion framework that learns both modality-specific and modality-invariant representations to fully exploit cross-modal complementarity. Li et al. [30] introduced a decoupled multimodal distillation approach that enhances the distinctiveness of each modality’s representation, thereby alleviating heterogeneity across modalities. Zhuang et al. [31] designed the Global-Local Modal (GLoMo) fusion framework, which leverages expert networks to automatically select and integrate key local representations from each modality while preserving global information during fusion. To reduce the reliance on large-scale labeled datasets, Li et al. [32] proposed a gradient-based active learning method with curriculum enhancement that strategically selects valuable samples from unlabeled data pools. Yuan et al. [33] presented the Multimodal Consistency-based Teacher (MC-Teacher), which applies a semi-supervised learning strategy to leverage unlabeled data and improve MER performance. Wang et al. [34] proposed a Disentangled-Language-Focused (DLF) framework for language-centered multimodal representation learning, introducing four geometric metrics to enhance disentanglement and further developing the Language-Focused Attractor (LFA), which uses language-guided cross-attention to enrich language representations with complementary modality-specific information. Yang et al. [35] introduced the Multimodal Sentiment Analysis and Emotion Recognition Adapter (MSE-Adapter), a lightweight plug-in that enables Large Language Models (LLMs) to perform MER tasks while retaining their general capabilities. Finally, Zhao et al. [36] proposed decomposing unimodal representations into emotion-specific and emotion-irrelevant features, using only the former to reduce interference from irrelevant information in MER tasks.

Despite advances in modeling cross-modal interactions, most fusion strategies implicitly assume semantic consistency across modalities and lack mechanisms to detect or resolve cross-modal conflicts. As a result, they are vulnerable to modality dominance and cannot ensure an accurate multimodal consensus when semantic inconsistencies occur.

B. Multi-task Learning

In recent years, researchers have increasingly focused on potential semantic inconsistencies between modalities in MER and have explored capturing both unimodal and multimodal representations simultaneously through multi-task learning.

Yu et al. [22] introduced the CH-SIMS dataset for Chinese sentiment analysis, which provides both multimodal and

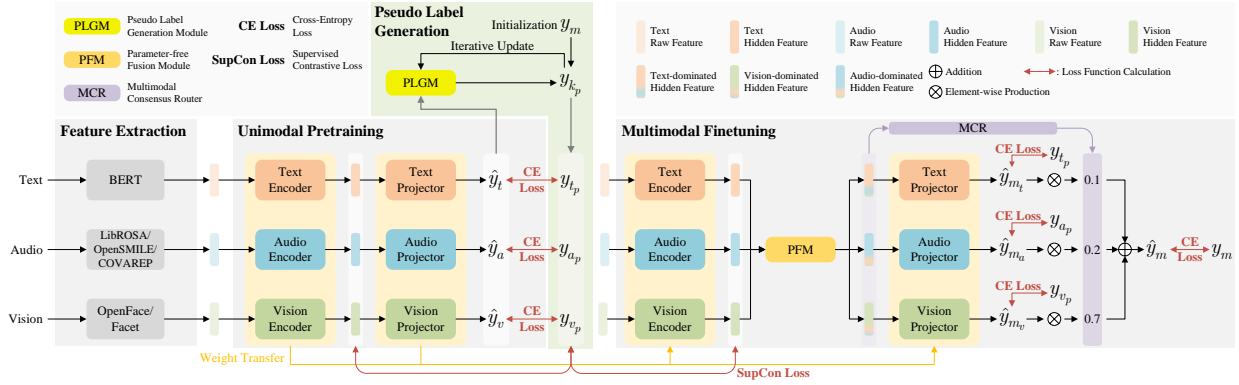


Fig. 2. The overall framework of the CMC model. CMC mainly comprises three core modules: the Pseudo Label Generation Module (PLGM), the Parameter-free Fusion Module (PFM), and the Multimodal Consensus Router (MCR). In the unimodal pretraining stage, the PLGM generates pseudo unimodal labels to enable self-supervised pretraining of unimodal models. During the multimodal finetuning stage, the hidden representations of each modality are fused through the PFM, after which the MCR assigns weights to each modality. Finally, these weights are applied to perform weighted fusion of the unimodal model predictions, producing the final emotion recognition results.

independent unimodal annotations, addressing the limitation of MER datasets containing only unified multimodal labels. They also proposed a late-fusion-based multi-task learning framework as a benchmark. Later, Yu et al. [37] developed a label generation module using self-supervised strategies to obtain unimodal supervision signals and jointly trained unimodal and multimodal tasks to capture both consistency and divergence. Liu et al. [38] highlighted the role of nonverbal cues in MER and released CH-SIMS v2, an extension of CH-SIMS. They further proposed the Acoustic Visual Mixup Consistent (AV-MC) framework, which combines audio and visual modalities from different videos to enhance the model's ability to interpret diverse nonverbal contexts for emotion recognition. Sun et al. [39] introduced the Sequential Fusion of Text-close and Text-far Representations (SFTTR) framework, designed to distill multimodal representations from text-close and text-far contexts. Luo et al. [40] proposed TriagedMSA to address emotional divergence across modalities, incorporating the Sentiment Disagreement Triage (SDT) network to distinguish between consistent and divergent samples, thereby reducing mutual interference. To handle these samples separately, they introduced the Sentiment Commonality Attention (SCA) and Sentiment Selection Attention (SSA) networks. In addition, they developed the Adaptive Polarity Detection (APD) algorithm to dynamically assess emotional consistency or divergence across modalities, ensuring generalization to datasets lacking unimodal labels.

Although multi-task frameworks incorporate unimodal supervision, most of them primarily aim to enrich representations rather than to calibrate multimodal consensus. And most models remain large and lack lightweight designs, which limits their applicability in resource-constrained settings.

III. METHOD

A. Problem Definition

The MER task aims to recognize human emotions from multiple modalities in video data, typically including text, audio, and vision. After feature extraction, we obtain text features $X_t \in \mathbb{R}^{l_t \times d_t}$, audio features $X_a \in \mathbb{R}^{l_a \times d_a}$, and visual

features $X_v \in \mathbb{R}^{l_v \times d_v}$, where l_t , l_a , and l_v denote the sequence lengths, and d_t , d_a , and d_v represent the feature dimensions of each modality. These modality-specific feature sequences X_t , X_a , and X_v are then input into a multimodal fusion encoder f_m to generate a joint multimodal representation $h_m = f_m(X_t, X_a, X_v)$. Finally, this representation h_m is passed to a multimodal classifier p_m , which outputs the final emotion prediction $\hat{y} = p_m(h_m)$.

In contrast to conventional MER formulations, we frame our problem as calibrating multimodal consensus: ensuring that the final decision reflects reliable contributions from all modalities while preventing any erroneous modality from dominating the others.

B. Overall Framework

In this section, we describe the forward propagation process of CMC, which comprises two training stages. The first stage pretrains individual unimodal models, and the second stage finetunes the fusion model to calibrate multimodal consensus. The overall architecture is illustrated in Fig. 2. The detailed implementations of the PLGM, PFM, and MCR modules are presented in the following subsections.

1) *Unimodal Pretraining*: For each modality sequence X_k ($k \in \{t, a, v\}$) obtained after feature extraction, we employ a unimodal encoder f_k ($k \in \{t, a, v\}$) to generate the corresponding unimodal representation \hat{h}_k :

$$\hat{h}_k = f_k(X_k) \in \mathbb{R}^{l_k \times B \times d} \quad (1)$$

where B denotes the batch size and d represents the dimensionality of the shared feature space, to which each modality sequence is projected via a one-dimensional convolution. The specific implementations of the unimodal encoder f_k for different modalities are as follows:

$$\begin{aligned} \hat{h}_t &= \text{Transformer}_t(\text{Conv1D}_t(X_t)) \\ \hat{h}_a &= \text{Transformer}_a(\text{Conv1D}_a(\text{BatchNorm1D}_a(X_a))) \\ \hat{h}_v &= \text{Transformer}_v(\text{Conv1D}_v(\text{BatchNorm1D}_v(X_v))) \end{aligned} \quad (2)$$

For the audio and visual sequences, we apply one-dimensional batch normalization before the one-dimensional

convolution to ensure numerical stability of the features. For the text sequence, since the features are extracted using BERT, batch normalization is unnecessary.

Subsequently, we average over the temporal dimension to obtain the utterance-level representation h'_k :

$$h'_k = \text{Average}(\hat{h}_k) \in \mathbb{R}^{B \times d} \quad (3)$$

To reduce heterogeneity across modalities, we normalize the utterance-level representation h'_k :

$$h_k = \frac{h'_k}{\|h'_k\|_2} \quad (4)$$

where $\|\cdot\|_2$ denotes the L2 norm. The normalized representations from each modality are then passed to their respective classifiers p_k to generate the predictions \hat{y}_k :

$$\hat{y}_k = p_k(h_k) \in \mathbb{R}^{B \times c} \quad (5)$$

where c is the number of classes. The classifier p_k is implemented as follows:

$$\begin{aligned} \bar{h}_k &= \text{Linear}(\text{Dropout}(\text{ReLU}(\text{Linear}(h_k)))) \in \mathbb{R}^{B \times d} \\ \hat{y}_k &= \text{Linear}(\bar{h}_k + h_k) \end{aligned} \quad (6)$$

Next, we employ the proposed PLGM to dynamically generate pseudo labels y_{k_p} , enabling self-supervised learning for unimodal models:

$$\begin{aligned} y_{k_p} &= \text{PLGM}(\hat{y}_k, y_{k_p}) \\ L_{\text{task}}^{\text{uni}} &= \sum_{k \in \{t, a, v\}} \text{CE}(\hat{y}_k, y_{k_p}) \end{aligned} \quad (7)$$

where y_{k_p} is initialized with y_m , the multimodal label at the start of training, and is iteratively updated in each training batch.

To enhance the alignment of representations from different modalities within a shared feature space, we encourage samples from the same class to be close to one another, while samples from different classes remain distant. To achieve this, we adopt the Supervised Contrastive (SupCon) Loss introduced by Khosla et al. [41] as an additional constraint:

$$L_{\text{supcon}} = \text{SupCon}([h_t; h_a; h_v], [y_t; y_a; y_v]) \quad (8)$$

where $[\cdot; \cdot; \cdot]$ denotes concatenation. Finally, the unimodal models are pretrained by jointly optimizing the two loss functions:

$$L_{\text{uni}} = L_{\text{task}}^{\text{uni}} + L_{\text{supcon}} \quad (9)$$

2) *Multimodal Finetuning*: In the unimodal pretraining step, we obtained a trained encoder f_k and classifier p_k for each modality. During multimodal finetuning, each modality sequence X_k is first passed through the corresponding encoder f_k to produce the unimodal representation \hat{h}_k . These representations are then averaged and normalized to form the utterance-level representation h_k (Eq. 4). To allow each modality to incorporate complementary information from other modalities while retaining its own core features, we introduce the PFM:

$$\begin{aligned} h_x &= [h_t, h_a, h_v] \in \mathbb{R}^{B \times 3 \times d} \\ \tilde{h}_x &= \text{PFM}(h_x) \in \mathbb{R}^{B \times 3 \times d} \end{aligned} \quad (10)$$

Next, we extract the representation of each modality from \tilde{h}_x to obtain $\tilde{h}_k \in \mathbb{R}^{B \times d}$. We then feed \tilde{h}_k into the pretrained classifier p_k to generate the prediction \hat{y}_{m_k} for each modality:

$$\hat{y}_{m_k} = p_k(\tilde{h}_k) \in \mathbb{R}^{B \times c} \quad (11)$$

Next, we aggregate the representations of the three modalities to form the utterance-level multimodal representation h_m :

$$h_m = \text{Sum}(\tilde{h}_x) \in \mathbb{R}^{B \times d} \quad (12)$$

To mitigate the dominance of the text modality in MER and reduce the risk of incorrect predictions, we propose the MCR, which computes the modality weight scores w_m (corresponding to text, audio, and vision modalities, constrained to sum to 1):

$$w_m = \text{MCR}(h_m) \in \mathbb{R}^{B \times 3} \quad (13)$$

From w_m , we extract the weight score for each modality, denoted as $w_k \in \mathbb{R}^{B \times 1}$.

Subsequently, we compute the final fused emotion prediction \hat{y}_m by performing a weighted sum of the modality weight scores and their corresponding prediction results:

$$\hat{y}_m = w_t \hat{y}_{m_t} + w_a \hat{y}_{m_a} + w_v \hat{y}_{m_v} \quad (14)$$

Multi-task Learning: To achieve joint optimization of unimodal models and multimodal fusion, we train the CMC model using a multi-task learning framework. First, the loss function for the multimodal task is computed based on the fused emotion prediction \hat{y}_m :

$$L_m = \text{CE}(\hat{y}_m, y_m) \quad (15)$$

where y_m denotes the multimodal label. To allow the unimodal encoder f_k and classifier p_k to adjust according to the fusion results from the PFM, we also compute the unimodal loss in MER:

$$L_k = \text{CE}(\hat{y}_{m_k}, y_{k_p}) \quad (16)$$

These two components jointly form the loss for the MER task:

$$L_{\text{task}}^{\text{multi}} = L_m + \sum_{k \in \{t, a, v\}} L_k \quad (17)$$

Furthermore, to maintain alignment of representations across modalities in the feature space, we adopt the Supervised Contrastive Loss during multimodal finetuning. The final multimodal finetuning objective is defined as:

$$L_{\text{multi}} = L_{\text{task}}^{\text{multi}} + L_{\text{supcon}} \quad (18)$$

C. Pseudo Label Generation Module

In this section, we introduce the proposed Pseudo Label Generation Module (PLGM). The PLGM leverages multimodal labels as a reference, evaluates recognition accuracy by incorporating the gradient norms of the model outputs, and updates pseudo labels using an Exponential Moving Average (EMA) to improve training stability.

At the beginning of training, we initialize the pseudo unimodal labels for each modality using the multimodal label:

$$\tilde{y}_{k_p}^{\text{soft}} = \text{OneHot}(y_m) \quad (19)$$

where $y_{k_p}^{soft}$ represents the soft unimodal label for modality k , and $\text{OneHot}(\cdot)$ denotes the conversion of the multimodal label y_m into the corresponding one-hot vector. The hard unimodal label for modality k is then obtained by applying the argmax operation:

$$y_{k_p} = \text{argmax} (y_{k_p}^{soft}) \quad (20)$$

To allow the model to refine the pseudo unimodal labels based on its own predictions during training, we first compute the gradient of the cross-entropy loss with respect to the model output \hat{y}_k . This gradient is used to evaluate the recognition quality of different samples in each modality k :

$$g_k = \text{Softmax} (\hat{y}_k) - \text{OneHot} (y_{k_p}) \quad (21)$$

To identify potentially adjustable labels, we compute the gradient norms of \hat{y}_k with respect to the one-hot representations of all possible classes:

$$\|g_{k_{cls}}\|_2 = \|\text{Softmax} (\hat{y}_k) - \text{OneHot}(cls)\|_2 \quad (22)$$

where cls denotes the class index ($cls = 0, \dots, c - 1$, with c being the total number of classes). Consequently, we obtain a set of gradient norms for all classes:

$$G_k = \{\|g_{k_0}\|_2, \dots, \|g_{k_{c-1}}\|_2\} \quad (23)$$

Next, we apply the argmin operation to determine the potential label $y_{k_p}^r$:

$$y_{k_p}^r = \text{argmin} (G_k) \quad (24)$$

It is important to note that $y_{k_p}^r$ and y_{k_p} may either coincide or differ. To further distinguish these cases, we categorize the dataset samples into three types: 1) **Easy samples** (correct label, clear semantics): $y_{k_p}^r$ is identical to y_{k_p} . In this case, the gradient norm between the model output \hat{y}_k and y_{k_p} is the smallest, indicating that the network's prediction is close to y_{k_p} .

2) **Hard samples** (correct label, ambiguous semantics): $y_{k_p}^r$ differs from y_{k_p} , but the gradient norms between \hat{y}_k and both $y_{k_p}^r$ and y_{k_p} are comparable, suggesting that the model's prediction is ambiguous.

3) **Incorrect samples** (incorrect label): $y_{k_p}^r$ differs from y_{k_p} . Here, the gradient norm between \hat{y}_k and $y_{k_p}^r$ is substantially smaller than that between \hat{y}_k and y_{k_p} , indicating that the original label y_{k_p} is erroneous and should be replaced by $y_{k_p}^r$.

To further quantify these three cases, we compute the fusion coefficient α_k between y_{k_p} and $y_{k_p}^r$ using the gradient norms:

$$\alpha_k = \frac{\|g_k\|_2 - \|g_k^r\|_2}{\|g_k\|_2 + \|g_k^r\|_2} \quad (25)$$

where

$$g_k^r = \text{Softmax} (\hat{y}_k) - \text{OneHot} (y_{k_p}^r) \quad (26)$$

Finally, using α_k , we fuse y_{k_p} and $y_{k_p}^r$ to obtain the refined soft label $y_{k_p}^{soft}$:

$$y_{k_p}^{soft} = (1 - \alpha_k) \text{OneHot} (y_{k_p}) + \alpha_k \text{OneHot} (y_{k_p}^r) \quad (27)$$

To ensure that the updates of pseudo unimodal labels remain smooth and avoid excessive oscillations that could compromise

training stability, we adopt the Exponential Moving Average (EMA) method for label updates:

$$\left(y_{k_p}^{soft} \right)^i \leftarrow m_{k_p} \left(y_{k_p}^{soft} \right)^{i-1} + (1 - m_{k_p}) \left(y_{k_p}^{soft} \right)^i \quad (28)$$

where i denotes the current iteration, and m_{k_p} is a hyperparameter that controls the retention of historical label information. Furthermore, to better preserve the optimal model during unimodal pretraining with pseudo labels and to mitigate overfitting to label noise (as pseudo labels are inherently imperfect), we also apply EMA to maintain an EMA version of the unimodal model, denoted as $\theta_{k_{ema}}^1$:

$$\theta_{k_{ema}}^i \leftarrow m_{k_{theta}} \theta_{k_{ema}}^{i-1} + (1 - m_{k_{theta}}) \theta_{k_{ema}}^i \quad (29)$$

where i again denotes the current iteration, and $m_{k_{theta}}$ is a hyperparameter that governs the retention of historical model parameters.

Finally, to stabilize pseudo label generation and model preservation in the later stages of training, the hyperparameters m_{k_p} and $m_{k_{theta}}$ are dynamically adjusted. Specifically, they are updated as follows, such that their values gradually approach 1 as the number of epochs increases:

$$m_{k_{\{p, \theta\}}}^E = 1 - \frac{1 - m_{k_{\{p, \theta\}}}^{E-1}}{E^{\gamma_{k_{\{p, \theta\}}}}} \quad (30)$$

where E denotes the current training epoch ($E \geq 1$), and $\gamma_{k_{\{p, \theta\}}}$ is a decay factor that controls the growth rate of $m_{k_{\{p, \theta\}}}$.

D. Parameter-free Fusion Module

In this section, we introduce the proposed Parameter-free Fusion Module (PFM). The PFM is constructed on the basis of cosine similarity and regulates the strength of information fusion across modalities by adjusting the temperature coefficient. This design ensures that, while facilitating information exchange among modalities, the unique semantics of each modality are preserved, thereby enhancing recognition accuracy.

Specifically, the input to the PFM is $h_x \in \mathbb{R}^{B \times 3 \times d}$, obtained by concatenating h_t , h_a , and h_v . Since each utterance-level representation h_k ($k \in \{t, a, v\}$) is already L2-normalized, the cosine similarity s between modalities can be directly computed via matrix multiplication:

$$s = h_x h_x' \in \mathbb{R}^{B \times 3 \times 3} \quad (31)$$

where $h_x' \in \mathbb{R}^{B \times d \times 3}$ represents the transpose of h_x with respect to the last two dimensions. To prevent excessive loss of modality-specific information during fusion, we adopt a temperature-based similarity score:

$$\beta = \text{Softmax} (s/\tau) \in \mathbb{R}^{B \times 3 \times 3} \quad (32)$$

where τ is a hyperparameter that regulates the preservation of each modality's information. Finally, the fused representation is obtained by multiplying the similarity score β with h_x :

$$\tilde{h}_x = \beta h_x \in \mathbb{R}^{B \times 3 \times d} \quad (33)$$

¹This EMA model is initialized as the composition of the original classifier p_k and encoder f_k , i.e., $\theta_{k_{ema}} = p_k \circ f_k$.

TABLE I
STATISTICS OF DATASETS

Datasets	Total	Training	Validation	Test
CH-SIMS	2,281	1,368 (669/699)	456 (217/239)	457 (239/218)
CH-SIMS v2 (supervised)	4,403	2,722 (1,476/1,246)	647 (339/308)	1,034 (487/547)
CMU-MOSI	2,199	1,284	229	686
CMU-MOSEI	22,856	16,326	1,871	4,659

"supervised" denotes the labeled version of CH-SIMS v2. The number on the **left** side of the "/" indicates the count of samples with **consistent** modality semantics, while the number on the **right** side of the "/" indicates the count of samples with **inconsistent** modality semantics. If no parentheses are provided, it means the dataset cannot distinguish whether modality semantics are consistent due to the absence of ground-truth unimodal labels.

For simplicity, all subsequent mentions of CH-SIMS v2 in this paper refer to the **labeled version**.

At this stage, each modality integrates information from the others while largely preserving its own characteristics, thereby offering more reliable references for subsequent MER fusion decisions.

E. Multimodal Consensus Router

In this section, we introduce the proposed Multimodal Consensus Router (MCR). The MCR computes confidence scores for each modality from the fused multimodal features and employs these scores to weight the modality-specific predictions. This process suppresses the dominance of any single modality and enhances robustness, particularly in scenarios involving semantic conflicts.

Specifically, to capture the global multimodal information of each sample and objectively evaluate the confidence of each modality, we first sum the three modality-specific representations in $\tilde{h}_x \in \mathbb{R}^{B \times 3 \times d}$, obtained from the PFM, to form the multimodal representation $h_m \in \mathbb{R}^{B \times d}$ (Eq. 12). We then pass h_m through a linear layer that projects it from d dimensions to 3 dimensions:

$$z_m = \text{Linear}(h_m) \in \mathbb{R}^{B \times 3} \quad (34)$$

The weights for each modality are then obtained using the Softmax function:

$$w_m = \text{Softmax}(z_m) \in \mathbb{R}^{B \times 3} \quad (35)$$

By assigning distinct weights to each modality, the model achieves more reliable multimodal consensus, thereby enhancing robustness, particularly in scenarios involving semantic inconsistencies.

IV. EXPERIMENTS

A. Experimental Setup

1) **Datasets:** To comprehensively evaluate the proposed CMC model, we conducted experiments on four widely used Chinese and English MER datasets: **CH-SIMS** [22], **CH-SIMS v2** [38], **CMU-MOSI** [42], and **CMU-MOSEI** [43]. The following provides a brief description of each dataset.

CH-SIMS [22]: A Chinese multimodal video emotion recognition dataset containing 2,281 clips collected from movies, TV dramas, and variety shows. Each clip includes multimodal annotations, independent unimodal annotations, and emotion intensity scores ranging from -1 (strongly negative) to +1 (strongly positive).

TABLE II
STATISTICS OF MODALITY FEATURES

Datasets	Modalities	Feature Extraction Tools	Sequence Length	Feature Dimension
CH-SIMS	Text	BERT-BASE	39	768
	Audio	LibROSA	400	33
	Vision	OpenFace	55	709
CH-SIMS v2	Text	BERT-BASE	50	768
	Audio	OpenSMILE	925	25
	Vision	OpenFace	232	177
CMU-MOSI	Text	BERT-BASE	50	768
	Audio	COVAREP	375	5
	Vision	Facet	500	20
CMU-MOSEI	Text	BERT-BASE	50	768
	Audio	COVAREP	500	74
	Vision	Facet	500	35

CH-SIMS v2 [38]: An extended version of CH-SIMS with 4,403 labeled and 10,161 unlabeled video clips. Like CH-SIMS, it provides emotion intensity scores ranging from -1 to +1. In this paper, only the labeled clips are used for training.

CMU-MOSI [42]: A benchmark dataset of YouTube movie review videos annotated across three modalities, text, vision, and audio. It consists of monologue-style videos where users express opinions on diverse topics. CMU-MOSI includes 2,199 opinion videos from 93 speakers, with emotion intensity scores ranging from -3 (strongly negative) to +3 (strongly positive).

CMU-MOSEI [43]: A large-scale multimodal video emotion recognition dataset comprising 22,856 opinion videos. Similar to CMU-MOSI, it provides emotion intensity scores ranging from -3 to +3.

The overall dataset statistics are summarized in Table I.

2) **Feature Extraction: Text:** Textual features are extracted and finetuned using the pretrained BERT_{BASE} [21].

Audio: For the CH-SIMS dataset, audio features are extracted with LibROSA [44], including log fundamental frequency (log F0), mel-frequency cepstral coefficients (MFCCs), and Constant-Q chroma (CQT) features. For the CH-SIMS v2 dataset, audio features are obtained using OpenSMILE [45], producing eGeMAPS Low-Level Descriptor (LLD) features. For the CMU-MOSI and CMU-MOSEI datasets, audio features are extracted with COVAREP [46], which primarily include quasi open quotient, normalized amplitude quotient, glottal source parameters, and other features.

Vision: For the CH-SIMS and CH-SIMS v2 datasets, visual features are extracted with OpenFace [47], covering facial landmarks, facial action units, head pose, head orientation, eye gaze, and other features. For the CMU-MOSI and CMU-MOSEI datasets, visual features are extracted with Facet².

The overall statistics of these modality features are summarized in Table II.

3) **Evaluation Metrics:** For the CH-SIMS and CH-SIMS v2 datasets, to investigate model performance under conditions of modality semantic inconsistency, we divided the test sets (D_{test}) into two subsets: modality semantic consistent (D_{msc}) and modality semantic inconsistent (D_{msi})³. Thus, $D_{\text{test}} =$

²iMotions 2017. <https://imotions.com/>

³Specifically, we classify test instances in which the multimodal label and the unimodal labels for text, audio, and visual all agree (i.e., all emotion intensity scores are >0 , or all $=0$, or all <0) as D_{msc} , and the remaining instances as D_{msi} .

TABLE III
HYPERPARAMETER SETTINGS

Settings	CH-SIMS	CH-SIMS v2	CMU-MOSI	CMU-MOSEI
Output Dropout	0.4	0.3	0.5	0.0
{Text, Audio, Vision} Attention Heads	4	2	4	4
{Text, Audio, Vision} Transformer Layers	5	4	2	2

$D_{msc} \cup D_{msi}$. We report binary classification accuracy (non-positive (≤ 0) vs. positive (> 0)) on these three test sets. For the CMU-MOSI and CMU-MOSEI datasets, we report binary classification accuracy Acc_2 (negative (< 0) vs. non-negative (≥ 0)) along with the corresponding F1 score.

Binary classification accuracy is calculated as:

$$Acc_2 = \frac{TP + TN}{TP + TN + FP + FN} \quad (36)$$

where TP denotes true positives, TN true negatives, FP false positives, and FN false negatives.

The *F1 Score*, defined as the harmonic mean of *Precision* and *Recall*, is computed as:

$$F1\ Score = \frac{2}{Precision^{-1} + Recall^{-1}} \quad (37)$$

where

$$Precision = \frac{TP}{TP + FP} \quad (38)$$

$$Recall = \frac{TP}{TP + FN}$$

4) *Implementation Details*: In our experiments, we applied grid search to optimize three hyperparameters, transformer layers, attention heads, and output dropout, while keeping all other parameters fixed. The search space was defined as follows: transformer layers {1, 2, 3, 4, 5}, attention heads {1, 2, 4, 8}, and output dropout {0.0, 0.1, 0.2, 0.3, 0.4, 0.5}.

To further constrain the hyperparameter search space, several parameters were fixed: the number of epochs was set to 100, early stopping patience to 10, batch size to 64, and the initial learning rate to 1e-3. The initial momentum for text pseudo labels $m_{t_p}^0$ was set to 0.8, and for audio and vision pseudo labels $m_{\{a,v\}_p}^0$ to 0.99. The decay factor for text, audio, and vision pseudo labels $\gamma_{\{t,a,v\}_p}$ was 0.5. The initial momentum of the EMA models was set to 0.8 for text ($m_{t_\theta}^0$), 0.9 for audio ($m_{a_\theta}^0$), and 0.6 for vision ($m_{v_\theta}^0$). The corresponding EMA decay factors were $\gamma_{t_\theta}=2.5$, $\gamma_{a_\theta}=5.0$, and $\gamma_{v_\theta}=2.0$.

The optimal hyperparameter configurations obtained for different datasets are reported in Table III.

All experiments were conducted on a single NVIDIA GeForce RTX 4090 D GPU. The random seed was fixed at 1111. The software environment consisted of Python 3.10 and PyTorch 2.7.1, with the Adam optimizer [48] used for training.

5) *Baselines*: To evaluate the effectiveness of the proposed CMC model, we compared it against several state-of-the-art methods: **Self-MM** [37], **AV-MC** [38], **EMT-DLFR** [13], **MC-Teacher** [33], **SFTTR** [39], **TriagedMSA** [40], **SDRS** [36], and **MSE-Adapter** [35].

B. Comparison with State-of-the-art Methods

To comprehensively evaluate the performance of the CMC model, we conducted experiments on four unaligned MER datasets: CH-SIMS, CH-SIMS v2, CMU-MOSI, and CMU-MOSEI, as summarized in Table IV. The results show that CMC achieves strong performance with fewer parameters and reaches state-of-the-art levels in most cases. It only slightly lags behind SDRS [36] on the CMU-MOSI dataset and behind MSE-Adapter [35] based on LLaMA2-7B and ChatGLM3-6B on the CMU-MOSEI dataset (while our method is built on the 0.1B BERT_{BASE}).

Specifically, on the full test set D_{test} of CH-SIMS, CMC improves binary classification accuracy by 2.11% over the previous best, SDRS. On the D_{msc} subset, it outperforms AV-MC [38] by 2.93%, and on the D_{msi} subset, it surpasses SFTTR [39] by 4.59%.

On the full test set D_{test} of CH-SIMS v2, CMC achieves a 0.10% improvement in binary classification accuracy over the previous best, MC-Teacher [33]⁴. On the D_{msc} subset, CMC outperforms MSE-ChatGLM3-6B by 0.82%, and on the D_{msi} subset, it surpasses MSE-ChatGLM3-6B by 1.65%.

The improvements on the semantically inconsistent subsets D_{msi} clearly demonstrate that CMC goes beyond simple feature fusion to establish a robust multimodal consensus that resists the misleading dominance of any single modality.

Although CMC does not achieve the best results on CMU-MOSI and CMU-MOSEI, it still delivers highly competitive performance. On CMU-MOSI, Acc_2 and F1 are only 0.37% and 0.38% lower than SDRS, respectively. On CMU-MOSEI, Acc_2 and F1 are both 2.45% lower than MSE-ChatGLM3-6B. However, the Pretrained Language Model (PLM) BERT_{BASE} used in CMC contains only about 1.67% of the parameters of ChatGLM3-6B, and the non-PLM components of CMC comprise only about 4.23% of those in MSE-ChatGLM3-6B.

These findings reveal a key limitation of prior MER methods: although many emphasize richer fusion architectures or incorporate auxiliary supervision, they largely overlook how consensus is established across modalities. Without explicit consensus calibration, models risk suppressing informative but weak modalities or being misled by dominant yet erroneous ones. In contrast, our experimental results show that CMC effectively calibrates multimodal consensus through PLGM, PFM, and MCR, thereby producing more accurate emotion predictions and achieving competitive performance.

C. Ablation Studies

To further evaluate the contribution of each proposed module, we conducted ablation studies on four datasets: CH-SIMS, CH-SIMS v2, CMU-MOSI, and CMU-MOSEI, as presented in Table V. In these experiments, we also introduced a variant of CMC in the multimodal finetuning stage (i.e., CMC-variant) and carried out corresponding analyses, as shown in Fig. 3.

As indicated in the table, for CMC, removing PLGM, PFM, or MCR generally results in reduced binary classification

⁴Note that MC-Teacher leverages **both** labeled data from CH-SIMS v2 and additional unlabeled data for semi-supervised training, whereas our method uses **only** labeled data from this dataset.

TABLE IV
COMPARISON WITH STATE-OF-THE-ART METHODS

Models	Years	CH-SIMS				CH-SIMS v2				CMU-MOSI			CMU-MOSEI		
		D _{test}	D _{msc}	D _{msi}	Size	D _{test}	D _{msc}	D _{msi}	Size	Acc2	F1	Size	Acc2	F1	Size
Self-MM [37]	2021	80.74	-	-	-	-	-	-	-	84.00	84.42	-	82.81	82.53	-
AV-MC* [38]	2022	-	-	-	-	82.50	-	-	-	-	-	-	-	-	-
EMT-DLFR [13]	2023	80.10	-	-	-	-	-	-	-	83.30	83.20	-	83.40	83.70	-
MC-Teacher [33]	2024	-	-	-	-	84.33	-	-	-	-	-	-	-	-	-
SFTTR [39]	2025	81.62	-	-	-	-	-	-	-	82.94	82.92	-	82.89	83.15	-
TriagedMSA [40]	2025	-	-	-	-	83.75	-	-	-	-	-	-	-	-	-
SDRS [36]	2025	82.79	-	-	-	-	-	-	-	84.77	84.70	-	84.37	84.27	-
MSE-Qwen-1.8B [35]	-	-	-	-	-	80.44	-	-	-	-	-	-	84.12	83.45	-
MSE-LLaMA2-7B [35]	2025	-	-	-	-	75.53	-	-	-	-	-	-	86.74	86.51	-
MSE-ChatGLM3-6B* [35]	-	-	-	-	-	83.77	-	-	-	-	-	-	86.91	86.77	-
Self-MM* [37]	2021	76.37	89.54	61.93	381,380	78.43	89.53	68.56	244,676	81.78	81.75	206,980	81.73	82.22	172,532
AV-MC* [38]	2022	79.21	91.21	66.06	76.162	81.62	91.17	73.13	66.442	78.13	78.07	63.256	81.03	81.32	64.768
EMT-DLFR* [13]	2023	78.34	89.96	65.60	1,525,592	78.63	90.14	68.37	1,439,164	82.51	82.38	2,322,779	74.31	75.49	2,115,583
SFTTR* [39]	2025	79.87	88.70	70.18	20,898,434	77.66	85.63	70.57	20,608,130	82.36	82.29	23,573,761	81.03	81.61	30,984,578
MSE-Qwen-1.8B* [35]	2025	69.15	73.64	64.22	1,539,992	79.50	87.89	71.85	1,400,268	45.92	30.42	1,331,660	82.12	81.15	1,351,244
MSE-LLaMA2-7B* [35]	2025	70.90	76.57	64.68	2,820,440	76.60	87.68	66.73	2,680,716	74.64	74.63	2,612,108	86.35	86.06	2,631,692
MSE-ChatGLM3-6B* [35]	78.77	87.87	68.81	2,820,440	83.17	93.43	74.04	2,680,716	82.94	82.76	2,612,108	86.59	86.19	2,631,692	
CMC (Ours)	-	84.90	94.14	74.77	247,096	84.43	94.25	75.69	190,624	84.40	84.32	108,382	84.46	84.32	111,238

The metric reported on CH-SIMS and CH-SIMS v2 is binary classification accuracy.

“Size” denotes the number of model parameters, excluding those of the pretrained language model (BERT or LLM).

“*” indicates results reproduced using open-source code.

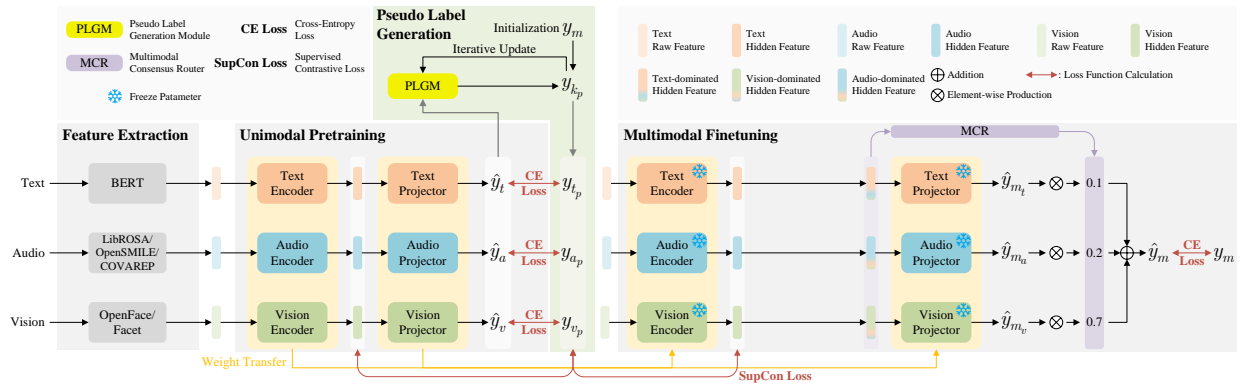


Fig. 3. The overall framework of the CMC-variant model. During the multimodal finetuning stage, the parameters of the Encoder f_k and Projector p_k for all modalities are frozen, the PFM is removed, and the training is conducted by optimizing only the MCR component in a single-task setting.

TABLE V
ABLATION STUDIES

Models	CH-SIMS				CH-SIMS v2				CMU-MOSI		CMU-MOSEI	
	D _{test}	D _{msc}	D _{msi}	Size	D _{test}	D _{msc}	D _{msi}	Size	Acc2	F1	Acc2	F1
CMC	84.90	94.14	74.77	84.43	94.25	75.69	84.40	84.32	84.46	84.32	84.46	84.32
w/o PLGM	80.96	86.61	74.77	83.17	92.40	74.95	82.65	82.41	83.41	83.65		
w/o PFM	83.59	92.05	74.31	81.62	90.97	73.31	82.94	82.97	84.12	84.06		
w/o MCR	82.49	92.47	71.56	82.69	89.94	76.23	82.80	82.63	83.90	83.60		
<i>The following are progressive experiments with variant forms:</i>												
single-task	80.74	89.54	71.10	82.98	93.02	74.04	82.80	82.75	83.97	84.07		
single-task w/o PFM	79.65	86.61	72.02	81.82	91.58	73.13	82.36	82.38	83.30	83.46		
CMC-variant	85.34	93.72	76.15	85.11	92.61	78.43	75.80	75.86	82.94	83.20		

The metric reported on CH-SIMS and CH-SIMS v2 is binary classification accuracy.

“single-task” indicates that, during the multimodal finetuning stage, only the multimodal label is used to compute the training loss.

“CMC-variant” refers to the variant forms of multimodal finetuning, as illustrated in Fig. 3.

accuracy. To further investigate the effect of multi-task optimization on unimodal models during multimodal finetuning, we removed the loss derived from unimodal labels and trained the model solely using multimodal labels. As shown in the “single-task” row, this setting leads to a substantial drop in binary classification accuracy. Moreover, to assess the impact of PFM under the single-task scenario, we removed PFM as

well. The “single-task w/o PFM” row demonstrates that this modification also causes a performance decline in most cases.

We further examined the performance of a variant that freezes all parameters except MCR under the single-task scenario without PFM, which represents the most intuitive model design. As shown in Fig. 3, the key difference between CMC and CMC-variant lies in whether the unimodal models

TABLE VI
NON-TEXTUAL MODALITY FEATURE QUALITY ASSESSMENT

Modality	CH-SIMS	CH-SIMS v2	CMU-MOSI	CMU-MOSEI
Audio	69.80	61.12	60.79	71.15
Vision	78.56	76.31	62.10	71.02

The metric reported on CH-SIMS, CH-SIMS v2, CMU-MOSI, and CMU-MOSEI is binary classification accuracy.

are frozen during multimodal finetuning. In CMC-variant, all unimodal models are frozen and only MCR is trained with multimodal labels. In contrast, in CMC, all unimodal models remain trainable, are equipped with the multimodal fusion module PFM, and are further optimized via multi-task learning.

From the “CMC-variant” row, it can be observed that this variant achieves the best binary classification accuracy on D_{test} and D_{msi} of CH-SIMS and CH-SIMS v2, even surpassing the original CMC. We attribute this to the uncertainty and noise introduced when multimodal labels are used to generate pseudo unimodal labels. By training only MCR during multimodal finetuning, CMC-variant reduces model degrees of freedom, thereby mitigating overfitting to noisy labels and acting as an implicit form of regularization. This enables superior performance on the semantically inconsistent subset D_{msi} , and consequently higher accuracy on the full test set D_{test} . However, CMC-variant does not outperform CMC on CMU-MOSI and CMU-MOSEI. We attribute this to the weaker representation of audio and visual features extracted with COVAREP and Facet in these datasets, which limits MCR’s ability to extract meaningful information from non-text modalities for calibrating multimodal consensus. In contrast, in CH-SIMS and CH-SIMS v2, both BERT-based textual features and OpenFace-based visual features exhibit stronger representational capacity, enabling MCR to perform more accurate multimodal consensus calibration.

To more clearly demonstrate the variability in non-textual modality quality across datasets, we conducted unimodal experiments on audio and visual inputs using CMC, as reported in Table VI. The results show that visual features extracted by OpenFace (CH-SIMS, CH-SIMS v2) outperform those extracted by Facet (CMU-MOSI, CMU-MOSEI), thereby providing richer information for multimodal consensus calibration in MCR.

Therefore, although CMC-variant is simpler and more intuitive, it is highly dependent on the quality of modality features. By contrast, while CMC requires training more parameters, it demonstrates greater robustness and reduced dependence on modality feature quality.

In conclusion, CMC effectively addresses the MER task through the PLGM, PFM, and MCR modules. The experiment with model variant suggests that pretraining unimodal models using PLGM and calibrating multimodal consensus with MCR are particularly promising, highlighting potential directions for future research.

TABLE VII
COMPARISON EXPERIMENTS WITH GROUND TRUTH UNIMODAL LABELS

Models	CH-SIMS			CH-SIMS v2		
	D_{test}	D_{msc}	D_{msi}	D_{test}	D_{msc}	D_{msi}
CMC	84.90	94.14	74.77	84.43	94.25	75.69
CMC-GT	85.56	92.89	77.52	84.33	92.40	77.15

The metric reported on CH-SIMS and CH-SIMS v2 is binary classification accuracy.

The suffix “-GT” denotes that ground truth unimodal labels are employed during unimodal pretraining.

V. DISCUSSIONS

A. Experiments under Groud Truth Unimodal Lables

To further evaluate the effectiveness of PLGM, we conducted comparative experiments on the CH-SIMS and CH-SIMS v2 datasets. During unimodal pretraining, we employed the ground truth unimodal labels provided by the datasets rather than the pseudo labels generated by PLGM, as shown in Table VII.

The results in the table show that using ground truth unimodal labels for pretraining yields higher binary classification accuracy on the modality semantic-inconsistent subset D_{msi} of both datasets. This improvement arises because more accurate labels enable finer optimization of each unimodal model. Consequently, during multimodal finetuning, the outputs \hat{y}_{m_k} ($k \in \{t, a, v\}$) of each unimodal model are more precise, leading to a more reliable multimodal consensus through MCR in scenarios with modality semantic inconsistency.

Furthermore, on the overall test set D_{test} of both datasets, using pseudo unimodal labels does not substantially affect performance. Notably, on the CH-SIMS v2 dataset, CMC achieves a binary classification accuracy 0.10% higher than that of CMC-GT, further confirming the reliability of the pseudo unimodal labels generated by PLGM.

B. Effect of Temperature on Modality Retention and Integration in PFM

To further investigate the effect of temperature on modality retention and integration in the PFM, and consequently on model performance, we adopted the configuration of Wang et al. [49] and conducted experiments on the CH-SIMS, CH-SIMS v2, CMU-MOSI, and CMU-MOSEI datasets. The experiments examined temperatures ranging from 0.05 to 1.0, as summarized in TableVIII.

As shown in the table, the model generally achieves optimal performance at a temperature of 0.07. For CMC, the best performance on the D_{msi} subset of CH-SIMS occurs at 0.05, whereas on the D_{msi} subset of CH-SIMS v2, it occurs at 0.7.

Overall, across all cases, the model performs better at temperatures below 1.0. This finding highlights the importance of preserving each modality’s intrinsic information in the PFM, without excessive interference from other modalities. Moreover, adopting a lower temperature such as 0.07 typically sharpens the Softmax distribution, thereby enhancing the model’s recognition capability.

TABLE VIII
ANALYSIS OF TEMPERATURES IN PFM

Temperatures	CH-SIMS			CH-SIMS v2			CMU-MOSI		CMU-MOSEI	
	D _{test}	D _{msc}	D _{msi}	D _{test}	D _{msc}	D _{msi}	Acc2	F1	Acc2	F1
0.07 (default)	84.90	94.14	74.77	84.43	94.25	75.69	84.40	84.32	84.46	84.32
0.05	84.68	92.47	76.15	81.62	90.97	73.31	82.80	82.72	84.33	84.20
0.1	82.06	92.05	71.10	82.11	91.58	73.67	83.38	83.24	84.14	84.18
0.2	81.18	87.87	73.85	82.21	92.40	73.13	83.38	83.25	83.67	83.75
0.3	83.15	89.96	75.69	82.69	91.79	74.59	81.20	81.17	82.38	82.54
0.4	82.71	90.79	73.85	82.40	92.40	73.49	83.38	83.33	83.52	83.38
0.5	81.84	89.96	72.94	81.33	89.73	73.86	82.51	82.22	83.07	83.02
0.6	78.99	89.54	67.43	83.08	91.79	75.32	83.24	83.15	82.85	83.05
0.7	82.71	92.05	72.48	83.95	92.40	76.42	83.24	83.17	83.19	83.35
0.8	81.18	89.96	71.56	82.21	90.76	74.59	83.24	83.22	83.86	84.01
0.9	81.18	90.38	71.10	82.01	90.76	74.22	83.67	83.61	83.22	83.37
1.0	81.40	89.54	72.48	82.79	91.17	75.32	81.49	81.50	84.27	84.31

The metric reported on CH-SIMS and CH-SIMS v2 is binary classification accuracy.

The range of temperature values is adopted from Wang et al. [49].

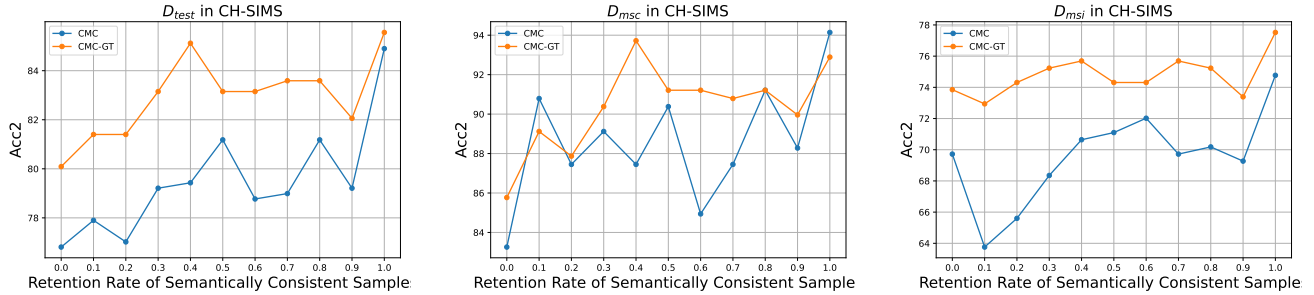


Fig. 4. Performance comparison between CMC and CMC-GT on various test sets of CH-SIMS. “CMC-GT” denotes that ground truth unimodal labels are employed during unimodal pretraining.

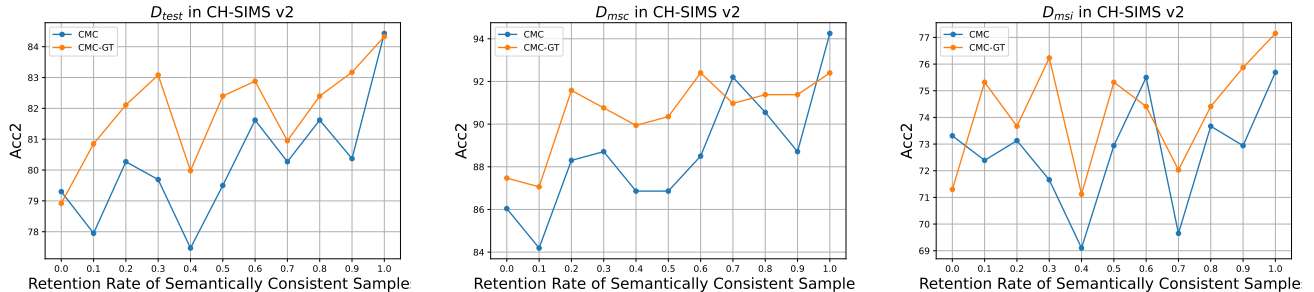


Fig. 5. Performance comparison between CMC and CMC-GT on various test sets of CH-SIMS v2. “CMC-GT” denotes that ground truth unimodal labels are employed during unimodal pretraining.

C. Effect of Semantic Consistency Ratio in Training Set

To further investigate why CMC outperforms CMC-GT on the D_{msc} subsets of the CH-SIMS and CH-SIMS v2 datasets (Table VII), we conducted experiments by varying the retention rate of modality semantically consistent samples in the training set, while keeping the validation and test sets unchanged. We then evaluated model performance on D_{test}, D_{msc}, and D_{msi} (Figs.4 and 5).

The results show that for the overall test set D_{test} and the modality semantically inconsistent subset D_{msi}, CMC-GT generally achieves higher binary classification accuracy than

CMC as the retention rate of modality semantically consistent samples increases, across both CH-SIMS and CH-SIMS v2. However, for the modality semantically consistent subset D_{msc}, the rate of improvement in CMC’s accuracy surpasses that of CMC-GT as the retention rate rises. To quantify this, we applied linear fitting using least squares: on D_{msc} of CH-SIMS, the slopes are 4.53 for CMC and 4.30 for CMC-GT; on CH-SIMS v2, the slopes are 6.77 for CMC and 4.02 for CMC-GT.

These findings suggest that CMC achieves higher accuracy than CMC-GT on D_{msc} (Table VII) because it relies exclusively on multimodal labels during training, which leads

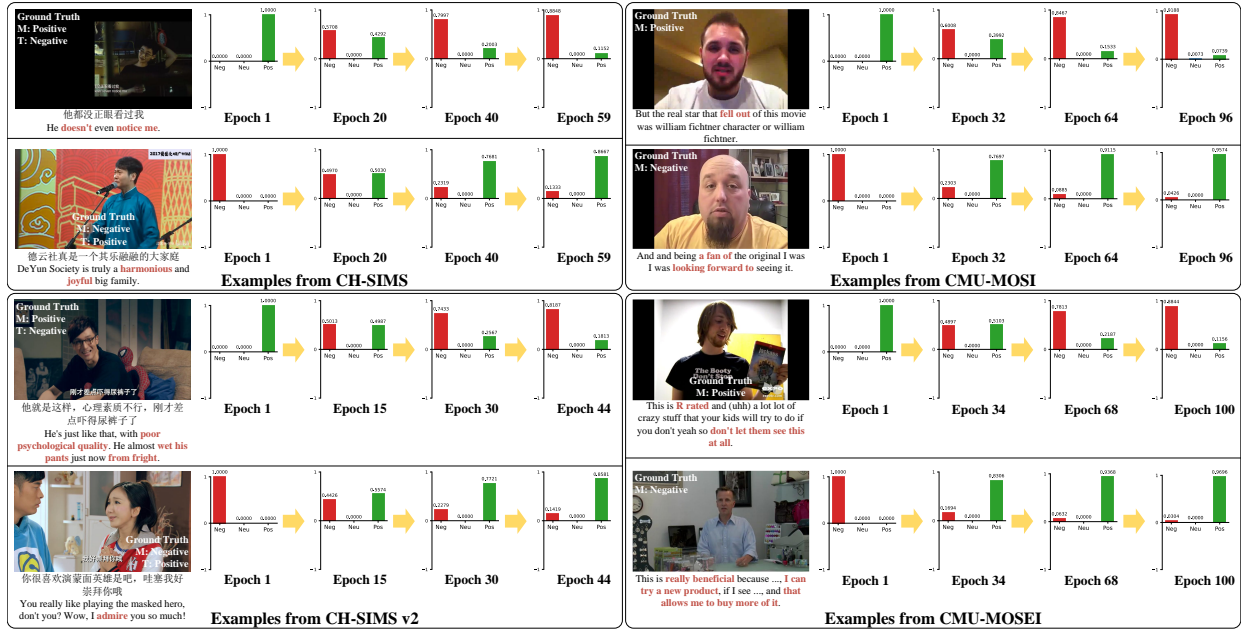


Fig. 6. Visualization of the text pseudo label generation process on the CH-SIMS, CH-SIMS v2, CMU-MOSI, and CMU-MOSEI datasets. Words highlighted in red denote emotion-related keywords. The labels “Neg”, “Neu”, and “Pos” correspond to Negative, Neutral, and Positive, respectively.

to overfitting on the relatively simpler modality semantically consistent samples. Consequently, as the retention rate of these samples increases, CMC’s accuracy improves more rapidly than that of CMC-GT.

In summary, CMC-GT performs better under modality semantic inconsistency, while CMC, relying on multimodal labels, shows faster improvement under modality semantic consistency. This indicates that although PLGM can effectively generate pseudo unimodal labels, the weaker representation capacity of non-text modalities constrains their quality, leaving the generated pseudo unimodal labels influenced by the biases of the initial multimodal labels.

D. Visualization of Pseudo Label Generation

To further demonstrate the effectiveness of PLGM, we visualized the pseudo label generation process for the text modality⁵ on the CH-SIMS, CH-SIMS v2, CMU-MOSI, and CMU-MOSEI datasets, as shown in Fig. 6.

As illustrated, in the CH-SIMS and CH-SIMS v2 datasets, phrases such as “doesn’t notice me” and “wet his pants” express negative emotions, enabling the model to revise the original “Positive” multimodal label into a “Negative” text unimodal label. Conversely, keywords such as “harmonious”, “joyful”, and “admire” convey positive emotions, allowing the model to adjust the original “Negative” multimodal label into a “Positive” text unimodal label.

For the CMU-MOSI and CMU-MOSEI datasets, which do not contain ground truth unimodal labels, PLGM can still

⁵Among the three modalities, text features extracted from pretrained language models exhibit stronger representational capacity than audio and visual features obtained using traditional tools. Consequently, text features are more reliable in generating accurate pseudo labels based on their own representations. Therefore, we select the text modality as a representative example to illustrate the effectiveness of PLGM.

effectively refine the original multimodal labels and generate accurate pseudo text unimodal labels. For instance, in CMU-MOSI, the phrase “fell out” conveys negative emotion, prompting the model to revise the “Positive” multimodal label to a “Negative” text unimodal label. Similarly, expressions such as “a fan of” and “looking forward to” indicate positive emotions, leading the model to adjust the “Negative” multimodal label to a “Positive” text unimodal label. In CMU-MOSEI, phrases such as “R rated” and “don’t let them see this at all” denote negative emotions, while “really beneficial” and “that allows me to buy more of it” reflect positive emotions. In both cases, PLGM successfully corrects the erroneous multimodal labels.

Overall, these experiments confirm that PLGM can efficiently and accurately correct mislabeled multimodal annotations by leveraging key emotional expressions in text. This correction is achieved in a simple, parameter-free manner, thereby generating high-quality pseudo unimodal labels to supervise unimodal model training.

E. Visualization of MCR in Calibrating Consensus

To further validate the effectiveness of MCR, we conducted visualization experiments on the CH-SIMS and CH-SIMS v2 datasets, as shown in Fig. 7.

The results indicate that MCR can accurately recognize human emotions in both cases of consistent and inconsistent modality semantics after adjustment. In particular, for samples with inconsistent modality semantics, even when the text modality conveys an opposite emotion, MCR still achieves correct recognition by preventing the text modality from dominating.

For instance, in the CH-SIMS dataset, words such as “intimidating” and “scary” in the text modality clearly express

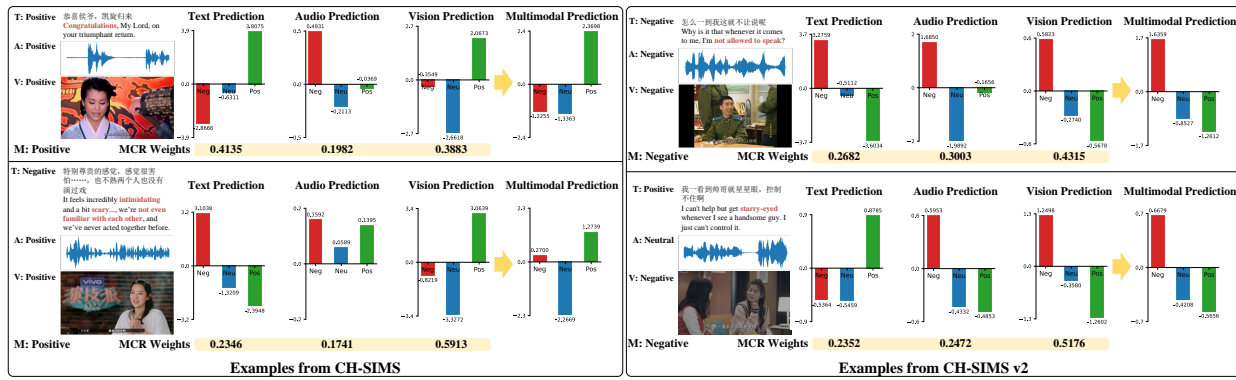


Fig. 7. Visualization of the MCR correction process on the CH-SIMS and CH-SIMS v2 datasets. Words highlighted in red denote emotion-related keywords. The labels “Neg”, “Neu”, and “Pos” correspond to Negative, Neutral, and Positive, respectively.

negative emotions. However, MCR assigns greater trust to the smiling vision modality and correctly identifies the video clip as positive. Similarly, in the CH-SIMS v2 dataset, the word “starry-eyed” in the text modality suggests a positive emotion, yet MCR relies more on the frowning vision modality and accurately classifies the clip as negative.

Moreover, we observed that the audio modality, which generally exhibits weaker representational capacity, occasionally makes incorrect predictions. Nevertheless, these errors rarely affect the final recognition, as MCR typically assigns lower confidence scores to the audio modality. This demonstrates the robustness of MCR in mitigating the influence of erroneous modalities.

Overall, MCR effectively calibrates multimodal consensus by adaptively assigning confidence scores to different modalities, thereby suppressing misleading inputs and ensuring accurate emotion recognition. Its robustness further enables it to reduce the negative impact of unreliable modalities.

VI. CONCLUSION

In summary, this paper introduces the CMC model to address the challenges of modality semantic inconsistency and text modality dominance in MER. By incorporating the PLGM, PFM, and MCR modules and adopting a two-stage multi-task training strategy, the model reduces the over-reliance on the text modality, guides the fusion process toward accurate multimodal consensus, and thereby enables more reliable recognition. For future work, we plan to integrate Multimodal Large Language Models (MLLMs) to enhance the representational capacity of non-text modalities and to explore pseudo label generation mechanisms based on model-wide gradient optimization to further improve model performance.

REFERENCES

- [1] A. Zadeh, M. Chen, S. Poria, E. Cambria, and L.-P. Morency, “Tensor fusion network for multimodal sentiment analysis,” in *Proc. Conf. Empirical Methods Natural Lang. Process.*, 2017, pp. 1103–1114.
- [2] Z. Liu, Y. Shen, V. B. Lakshminarasimhan, P. P. Liang, A. B. Zadeh, and L.-P. Morency, “Efficient low-rank multimodal fusion with modality-specific factors,” in *Proc. Assoc. Comput. Linguistics*, 2018, pp. 2247–2256.
- [3] Y. Wang, Y. Shen, Z. Liu, P. P. Liang, A. Zadeh, and L.-P. Morency, “Words can shift: Dynamically adjusting word representations using nonverbal behaviors,” in *Proc. AAAI Conf. Artif. Intell.*, vol. 33, no. 01, 2019, pp. 7216–7223.
- [4] R. Huan, G. Zhong, P. Chen, and R. Liang, “Trisat: Trimodal representation learning for multimodal sentiment analysis,” *IEEE/ACM Trans. Audio Speech Lang. Process.*, 2024.
- [5] P. Ouyang, J. Chen, Q. Ma, Z. Wang, and C. Bai, “Distinguishing visually similar images: Triplet contrastive learning framework for image-text retrieval,” in *Proc. IEEE Int. Conf. Multimedia Expo.* IEEE, 2024, pp. 1–6.
- [6] P. Ouyang, Q. Ma, and C. Bai, “Sparse information perception network for remote sensing cross-modal retrieval,” *IEEE Trans. Geosci. Remote Sens.*, 2025.
- [7] Y. Fang, W. Huang, G. Wan, K. Su, and M. Ye, “Emoe: Modality-specific enhanced dynamic emotion experts,” in *Proc. IEEE Conf. Comput. Vis. Pattern Recognit.*, 2025, pp. 14 314–14 324.
- [8] Q. Shi, M. Ye, W. Huang, B. Du, and X. Zong, “Gradient and structure consistency in multimodal emotion recognition,” *IEEE Trans. Image Process.*, 2025.
- [9] H. Pham, P. P. Liang, T. Manzini, L.-P. Morency, and B. Póczos, “Found in translation: Learning robust joint representations by cyclic translations between modalities,” in *Proc. AAAI Conf. Artif. Intell.*, vol. 33, no. 01, 2019, pp. 6892–6899.
- [10] Z. Wang, Z. Wan, and X. Wan, “Transmodality: An end2end fusion method with transformer for multimodal sentiment analysis,” in *Proc. Web Conf.*, 2020, pp. 2514–2520.
- [11] J. Tang, K. Li, X. Jin, A. Cichocki, Q. Zhao, and W. Kong, “Ctnf: Hierarchical learning for multimodal sentiment analysis using coupled-translation fusion network,” in *Proc. Assoc. Comput. Linguistics*, 2021, pp. 5301–5311.
- [12] Z. Yuan, W. Li, H. Xu, and W. Yu, “Transformer-based feature reconstruction network for robust multimodal sentiment analysis,” in *Proc. ACM Int. Conf. Multimedia*, 2021, pp. 4400–4407.
- [13] L. Sun, Z. Lian, B. Liu, and J. Tao, “Efficient multimodal transformer with dual-level feature restoration for robust multimodal sentiment analysis,” *IEEE Trans. Affective Comput.*, vol. 15, no. 1, pp. 309–325, 2023.
- [14] Z. Lian, L. Chen, L. Sun, B. Liu, and J. Tao, “Gcnet: Graph completion network for incomplete multimodal learning in conversation,” *IEEE Trans. Pattern Anal. Mach. Intell.*, vol. 45, no. 7, pp. 8419–8432, 2023.
- [15] R. Huan, G. Zhong, P. Chen, and R. Liang, “Unimf: A unified multimodal framework for multimodal sentiment analysis in missing modalities and unaligned multimodal sequences,” *IEEE Trans. Multimedia*, vol. 26, pp. 5753–5768, 2023.
- [16] T. Sun, W. Wang, L. Jing, Y. Cui, X. Song, and L. Nie, “Counterfactual reasoning for out-of-distribution multimodal sentiment analysis,” in *Proc. ACM Int. Conf. Multimedia*, 2022, pp. 15–23.
- [17] D. Yang, M. Li, D. Xiao, Y. Liu, K. Yang, Z. Chen, Y. Wang, P. Zhai, K. Li, and L. Zhang, “Towards multimodal sentiment analysis debiasing via bias purification,” in *Proc. Eur. Conf. Comput. Vis.* Springer, 2024, pp. 464–481.
- [18] T. Sun, J. Ni, W. Wang, L. Jing, Y. Wei, and L. Nie, “General debiasing for multimodal sentiment analysis,” in *Proc. ACM Int. Conf. Multimedia*, 2023, pp. 5861–5869.

[19] L. Ma, J. Li, D. Shao, J. Yan, J. Wang, and Y. Yan, "Bcd-mm: Multimodal sentiment analysis model with dual-bias-aware feature learning and attention mechanisms," *IEEE Access*, 2024.

[20] R. Huan, G. Zhong, P. Chen, and R. Liang, "Muldef: A model-agnostic debiasing framework for robust multimodal sentiment analysis," *IEEE Trans. Multimedia*, 2024.

[21] J. Devlin, M.-W. Chang, K. Lee, and K. Toutanova, "Bert: Pre-training of deep bidirectional transformers for language understanding," in *Proc. Conf. North Amer. Chapter Assoc. Comput. Linguistics*, 2019, pp. 4171–4186.

[22] W. Yu, H. Xu, F. Meng, Y. Zhu, Y. Ma, J. Wu, J. Zou, and K. Yang, "Ch-sims: A chinese multimodal sentiment analysis dataset with fine-grained annotation of modality," in *Proc. Assoc. Comput. Linguistics*, 2020, pp. 3718–3727.

[23] Y.-H. H. Tsai, S. Bai, P. P. Liang, J. Z. Kolter, L.-P. Morency, and R. Salakhutdinov, "Multimodal transformer for unaligned multimodal language sequences," in *Proc. Assoc. Comput. Linguistics*, vol. 2019, 2019, p. 6558.

[24] A. Vaswani, N. Shazeer, N. Parmar, J. Uszkoreit, L. Jones, A. N. Gomez, Ł. Kaiser, and I. Polosukhin, "Attention is all you need," in *Proc. Adv. Neural Inf. Process. Syst.*, vol. 30, 2017.

[25] F. Lv, X. Chen, Y. Huang, L. Duan, and G. Lin, "Progressive modality reinforcement for human multimodal emotion recognition from unaligned multimodal sequences," in *Proc. IEEE Conf. Comput. Vis. Pattern Recognit.*, 2021, pp. 2554–2562.

[26] T. Liang, G. Lin, L. Feng, Y. Zhang, and F. Lv, "Attention is not enough: Mitigating the distribution discrepancy in asynchronous multimodal sequence fusion," in *Proc. IEEE Int. Conf. Comput. Vis.*, 2021, pp. 8148–8156.

[27] J. Cheng, I. Fostiroopoulos, B. Boehm, and M. Soleymani, "Multimodal phased transformer for sentiment analysis," in *Proc. Conf. Empirical Methods Natural Lang. Process.*, 2021, pp. 2447–2458.

[28] J. Guo, J. Tang, W. Dai, Y. Ding, and W. Kong, "Dynamically adjust word representations using unaligned multimodal information," in *Proc. ACM Int. Conf. Multimedia*, 2022, pp. 3394–3402.

[29] D. Yang, H. Kuang, S. Huang, and L. Zhang, "Learning modality-specific and-agnostic representations for asynchronous multimodal language sequences," in *Proc. ACM Int. Conf. Multimedia*, 2022, pp. 1708–1717.

[30] Y. Li, Y. Wang, and Z. Cui, "Decoupled multimodal distilling for emotion recognition," in *Proc. IEEE Conf. Comput. Vis. Pattern Recognit.*, 2023, pp. 6631–6640.

[31] Y. Zhuang, Y. Zhang, Z. Hu, X. Zhang, J. Deng, and F. Ren, "Glomo: Global-local modal fusion for multimodal sentiment analysis," in *Proc. ACM Int. Conf. Multimedia*, 2024, pp. 1800–1809.

[32] X. Li, W. Ye, Y. Zhang, and X. Sun, "Grace: Gradient-based active learning with curriculum enhancement for multimodal sentiment analysis," in *Proc. ACM Int. Conf. Multimedia*, 2024, pp. 5702–5711.

[33] Z. Yuan, J. Fang, H. Xu, and K. Gao, "Multimodal consistency-based teacher for semi-supervised multimodal sentiment analysis," *IEEE/ACM Trans. Audio Speech Lang. Process.*, 2024.

[34] P. Wang, Q. Zhou, Y. Wu, T. Chen, and J. Hu, "Dlf: Disentangled-language-focused multimodal sentiment analysis," in *Proc. AAAI Conf. Artif. Intell.*, vol. 39, no. 20, 2025, pp. 21180–21188.

[35] Y. Yang, X. Dong, and Y. Qiang, "Mse-adapter: A lightweight plugin endowing llms with the capability to perform multimodal sentiment analysis and emotion recognition," in *Proc. AAAI Conf. Artif. Intell.*, vol. 39, no. 24, 2025, pp. 25642–25650.

[36] S. Zhao, Z. Yang, H. Shi, X. Feng, L. Meng, B. Qin, C. Yan, J. Tao, and G. Ding, "Sdrs: Sentiment-aware disentangled representation shifting for multimodal sentiment analysis," *IEEE Trans. Affective Comput.*, 2025.

[37] W. Yu, H. Xu, Z. Yuan, and J. Wu, "Learning modality-specific representations with self-supervised multi-task learning for multimodal sentiment analysis," in *Proc. AAAI Conf. Artif. Intell.*, vol. 35, no. 12, 2021, pp. 10790–10797.

[38] Y. Liu, Z. Yuan, H. Mao, Z. Liang, W. Yang, Y. Qiu, T. Cheng, X. Li, H. Xu, and K. Gao, "Make acoustic and visual cues matter: Ch-sims v2. 0 dataset and av-mixup consistent module," in *Proc. Int. Conf. Multimodal Interact.*, 2022, pp. 247–258.

[39] K. Sun and M. Tian, "Sequential fusion of text-close and text-far representations for multimodal sentiment analysis," in *Proc. Int. Conf. Comput. Linguistics*, 2025, pp. 40–49.

[40] Y. Luo, W. Liu, Q. Sun, S. Li, J. Li, R. Wu, and X. Tang, "Triagedmsa: Triaging sentimental disagreement in multimodal sentiment analysis," *IEEE Trans. Affective Comput.*, 2025.

[41] P. Khosla, P. Teterwak, C. Wang, A. Sarna, Y. Tian, P. Isola, A. Maschinot, C. Liu, and D. Krishnan, "Supervised contrastive learning," vol. 33, 2020, pp. 18661–18673.

[42] A. Zadeh, R. Zellers, E. Pincus, and L.-P. Morency, "Multimodal sentiment intensity analysis in videos: Facial gestures and verbal messages," *IEEE Intell. Syst.*, vol. 31, no. 6, pp. 82–88, 2016.

[43] A. B. Zadeh, P. P. Liang, S. Poria, E. Cambria, and L.-P. Morency, "Multimodal language analysis in the wild: Cmu-mosei dataset and interpretable dynamic fusion graph," in *Proc. Assoc. Comput. Linguistics*, 2018, pp. 2236–2246.

[44] B. McFee, C. Raffel, D. Liang, D. P. Ellis, M. McVicar, E. Battenberg, and O. Nieto, "librosa: Audio and music signal analysis in python." *SciPy*, vol. 2015, pp. 18–24, 2015.

[45] F. Eyben, M. Wöllmer, and B. Schuller, "Opensmile: the munich versatile and fast open-source audio feature extractor," in *Proc. ACM Int. Conf. Multimedia*, 2010, pp. 1459–1462.

[46] G. Degottex, J. Kane, T. Drugman, T. Raitio, and S. Scherer, "Covarep—a collaborative voice analysis repository for speech technologies," in *Proc. IEEE Int. Conf. Acoust. Speech Signal Process.* IEEE, 2014, pp. 960–964.

[47] T. Baltrušaitis, P. Robinson, and L.-P. Morency, "Openface: an open source facial behavior analysis toolkit," in *Proc. Winter Conf. Appl. Comput. Vis.* IEEE, 2016, pp. 1–10.

[48] D. P. Kingma and J. Ba, "Adam: A method for stochastic optimization," *arXiv preprint arXiv:1412.6980*, 2014.

[49] F. Wang and H. Liu, "Understanding the behaviour of contrastive loss," in *Proc. IEEE Conf. Comput. Vis. Pattern Recognit.*, 2021, pp. 2495–2504.